

Crystalline hydrogenation of graphene by STM tip-induced field dissociation of H₂

S. J. Tjung¹, S. M. Hollen², G. A. Gambrel¹, N. M. Santagata¹, E. Johnston-Halperin¹, J.A. Gupta^{1*}

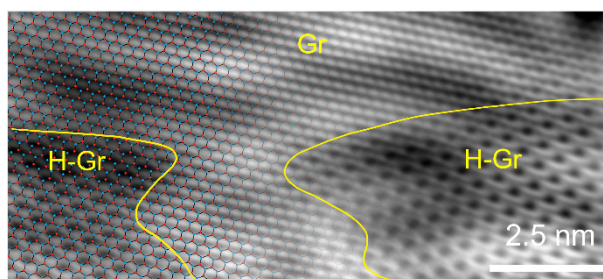
¹*Department of Physics, The Ohio State University, Columbus, OH 43210*

²*Department of Physics, University of New Hampshire, Durham, NH 03824*

Abstract

We have developed a novel method for crystalline hydrogenation of graphene on the nanoscale. Molecular hydrogen was physisorbed at 5 K onto pristine graphene islands grown on Cu(111) in ultrahigh vacuum. Field emission local to the tip of a scanning tunneling microscope dissociates H₂ and results in hydrogenated graphene. Atomically resolved images show a $\sqrt{3} \times \sqrt{3} R30^\circ$ reconstruction with respect to the graphene lattice, with hydrogen atoms on only one of the carbon sublattices. Tunneling spectroscopy shows a decrease in conductance on hydrogenated graphene, but no clear evidence of a wide band gap. The hydrogenation can be reversed by imaging with higher bias voltage.

Keywords: STM, hydrogenation, crystalline, graphane, field dissociation, quantum diffusion



*Corresponding author: jgupta@physics.osu.edu

Hydrogenation is of considerable interest for tuning graphene's electronic, magnetic, and chemical properties for a broad range of applications^{1,2}. Crystalline ordering would help in identifying the intrinsic properties of hydrogenated graphene and mitigating effects of disorder on, for example, carrier mobility in electronic transport. Currently, the evidence for ordered hydrogenated graphene and graphane (fully hydrogenated graphene) is structurally lacking. Most reports of hydrogenated graphene with chemical³⁻⁶, plasma⁷⁻¹⁰ or thermal cracker¹¹⁻²³ sources indicate electronic changes toward a band insulator^{6,8,10,11,14,15,17,23} but little or no evidence for crystalline order. In STM experiments on hydrogenated graphene on Ir(111), some ordering of H clusters was observed commensurate with the Gr/Ir Moiré pattern¹⁷. More recently, small ($\sim \text{nm}^2$) patches of ordered, hydrogen-related structures were observed after exposing CVD grown graphene on polycrystalline Cu foil to a hydrogen plasma²². Overall, there still seems to be a disconnect between theoretical expectations, which predict ordered, uniform H coverage^{24,25}, and experimental observations.

Here we report a new, *in situ* method for hydrogenation of graphene that results in crystalline order. Atomic hydrogen was produced by dissociating physisorbed H₂ at low temperature (5K) in the strong electric field local to a scanning tunneling microscope (STM) tip. We observe a $\sqrt{3} \times \sqrt{3}R30^\circ$ surface which we attribute to one hydrogen atom per carbon hexagon. STM images provide evidence for slow growth dynamics that may be limited by interactions between the hydrogenated graphene and residual physisorbed H₂. STM spectroscopy suggests a small suppression in conductivity that could indicate the opening of a bandgap, but interactions with the substrate may mask more significant changes in electronic structure. We found that pristine graphene could be recovered by imaging at higher bias voltages, suggesting that this hydrogenation method may be useful for patterning graphene's surface electronic structure in future devices.

Graphene islands were grown on Cu(111) by thermal decomposition of ethylene in ultrahigh vacuum (UHV) at a base pressure of $\sim 10^{-10}$ mbar²⁶⁻²⁸. A clean Cu(111) surface was first prepared by cycles of Ar⁺ sputtering and annealing at 600 °C, repeated until surface contamination was minimized in Auger electron spectra. Graphene was grown by introducing 2×10^{-5} mbar of ethylene gas into the UHV chamber while cycling the sample temperature 2-4 times from room temperature to $\sim 950^\circ \text{C}$. The sample was immediately transferred into the STM and cooled down to 5K within 6 hours. This method produces pristine graphene islands with an average coverage < 0.25 monolayers which can be studied by STM without any exposure to air^{26,27}.

All measurements were made with a CreaTec LT-STM operating at 5K. Constant current STM images were collected with a PtIr or a W tip. Tunneling spectroscopy was performed at fixed tip height by adding a 5-10 mV modulation at ~ 1000 Hz to the bias voltage. A lock-in amplifier then recorded the corresponding modulation in tunneling current, dI/dV , which provides information on the sample's local density of states (LDOS). STM images were calibrated using atomically resolved images of the Cu(111) surface. Image analysis was performed with the WSxM software²⁹.

Hydrogen functionalization of graphene was achieved by *in situ* field-emission dissociation of H₂ by the STM tip (Fig. 1a). A precision leak valve admits H₂ into the STM chamber at a pressure of 10^{-7} mbar for 5-10 min. Small holes in the radiation shields surrounding the STM allow some of the H₂ to adsorb onto the sample surface at 5 K³⁰. Dissociative adsorption of H₂ on Cu(111) has a significant activation barrier (~ 0.4 eV)^{31,32}, so that under these conditions, H₂ is only weakly bound to the surface (physisorption). STM images discussed below suggest a coverage of ~ 1 monolayer,

but the mobility of physisorbed H_2 on the surface makes a precise estimate difficult. To dissociate H_2 , we retract the tip by ~ 130 nm from the surface and apply a voltage of 50-120 V to maintain a field emission current of 0.5 nA for 5-10 min. These high energy electrons dissociate a fraction of the H_2 into atomic H, which can then interact with the graphene. Both cut and etched tips were used to qualitatively study how the tip shape influences the electric field profile for the field dissociation process.

As a baseline for comparison, an STM image of a pristine graphene island is shown in Fig 1b. Graphene islands (upper right half of image) are readily distinguished from the Cu(111) surface (lower left) by the greatly reduced density of point defects²⁶. We typically observe two kinds of point defects on the graphene island, both of which are imaged as depressions by STM: the smaller and fainter defects are from impurities trapped between the graphene and Cu(111) substrate, while the larger and darker dark defects may be a defect cluster in the graphene²⁷. Ripples due to scattering of electrons in the Cu(111) Shockley surface state can be seen on the graphene island and have been studied previously²⁶. A Fast Fourier Transform (FFT) of the indicated area in Fig. 1b shows a circular ring due to the surface state scattering. Atomic resolution imaging is sensitive to the STM tip termination, and though not resolved in Fig. 1b, other images of this island showed a Moiré pattern consistent with the smaller 2.46 Å graphene honeycomb lattice oriented at 0° with respect to the underlying 2.55 Å Cu(111) lattice (c.f., Supporting

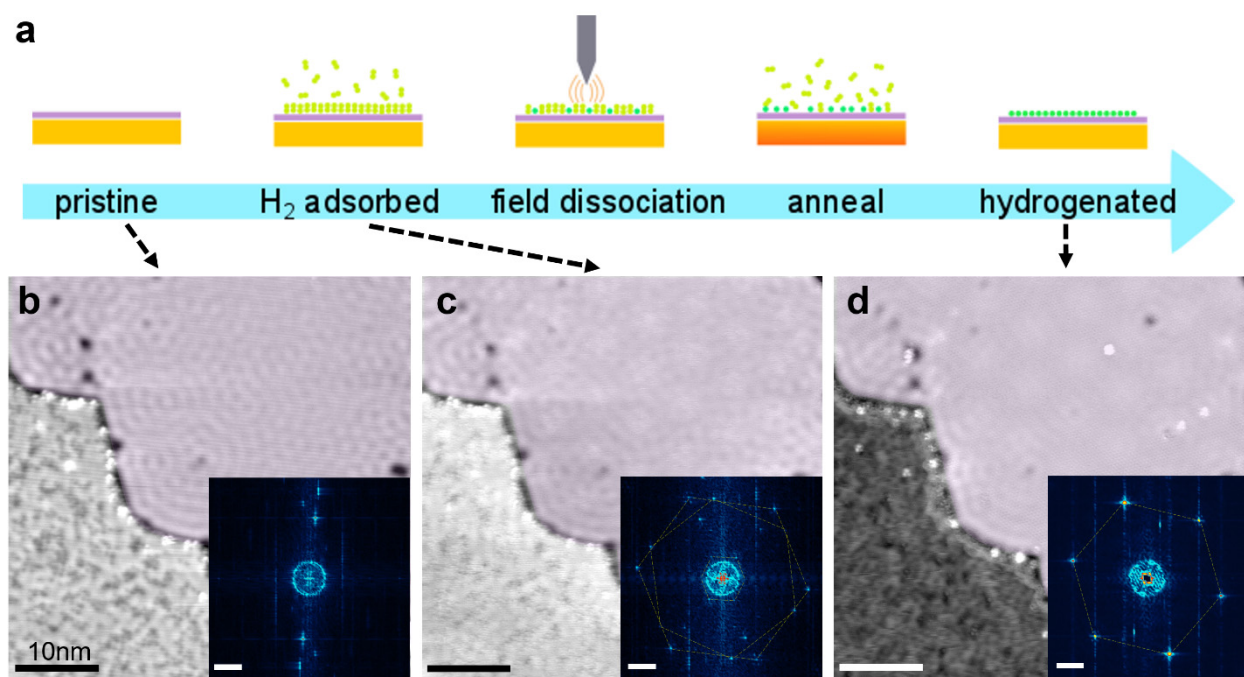


Figure 1. (a) Illustration of process to hydrogenate graphene. (b) STM image of the pristine graphene island (colored lavender) grown on Cu(111). (inset) FFT showing a circular ring from scattering of the Cu(111) surface state electrons. (c) STM image of the same island after H_2 deposition on the surface. Monolayer coverage is suggested by the appearance of H_2 lattices. The FFT (inset) shows multiple hexagonal spot patterns indicated by the yellow dashed lines and attributed to H_2 . (d) STM image after field dissociation and desorption of H_2 at 20 K, revealing a hexagonal lattice with 4.3Å spacing on the graphene island. The FFT (inset) confirms this lattice, and removal of H_2 -related structures. The Cu area appears darker than in (b,c) due to atomic H on the surface. $V = 50$ mV, $I = 0.2$ nA. FFT scale bar = 1.0 nm⁻¹.

Information). Due to the relatively weak Cu/graphene interaction, we observed a variety of Moiré patterns in imaging of other islands, consistent with various rotation angles with respect to the substrate.

Figure 1c shows the same graphene island after exposure to H₂. The motion of physisorbed H₂ at 5 K prevents imaging of isolated molecules with STM³⁰. However, a stable 3.6 Å triangular lattice is observed on both the graphene island and Cu(111) substrate, consistent with previous studies of physisorbed H₂ at monolayer coverage³⁰. FFT analysis of this image reveals additional periodic structures that are not readily apparent from the real space image. Other hexagons in the FFT correspond to lattice constants of 4.0 Å, 5.2 Å, and 10 Å and exhibit distinct rotational orientations. These are observed on the H₂/Cu(111) surface as well, but not on the pristine Cu or graphene surfaces. These additional lattices could be due to different domains or multiple layers of condensed H₂. The Moiré pattern associated with the gr/Cu surface is more evident with the tunneling tip in Fig. 1c, and we confirmed that it is unchanged upon H₂ adsorption.

We next performed field emission to produce atomic H on the surface. In contrast to physisorbed H₂, individual H atoms are more strongly chemisorbed on the surface and can be imaged with STM^{33,32}. In control experiments on H₂/Cu(100) (c.f., Supporting Information), we observed isolated point defects that we attribute to atomic H³³, together with the triangular 3.6 Å lattice structure consistent with monolayer coverage of physisorbed H₂³⁰. The H₂ could be desorbed by warming the STM stage up to 20 K³⁰, leaving the atomic H on the surface. On Cu(111), we also observed isolated point defects following field dissociation and desorption of physisorbed H₂ (Fig. 1d, bottom left corner). These defects can only be stably imaged by STM at lower bias voltages < 100 mV; the ‘streaky’ appearance on the Cu region in Fig. 1d reflects motion of the adsorbates induced by the tip while scanning (c.f., Supporting Information). Similar behavior has recently been reported for atomic H on Cu(111)³², and we similarly assign these defects to chemisorbed atomic hydrogen. We verified that atomic hydrogen is only produced if we field emit on the H₂ covered surface; field emission on clean Cu(111) occasionally produces point defects, but not the high density shown in Fig. 1c. These observations indicate that the field dissociation method can be used to produce atomic H *in situ* on the surface.

After field dissociation and desorption of H₂ via warming to 20 K, atomic resolution STM images of the graphene island show a new hexagonal lattice with a lattice constant of 4.3 Å, visible also in the corresponding FFT (Fig 1d). This new structure is only observed on the graphene island, and not on Cu(111). Discussed further below, this spacing is consistent with a $\sqrt{3} \times \sqrt{3}R30^\circ$ surface reconstruction of graphene. A few point defects are also created, but there are no larger scale defects in the hydrogenated graphene island. The Moiré pattern remains visible in both the real-space and FFT images, and is unchanged from the pristine graphene. Standing wave patterns associated with the underlying Cu Shockley state electron scattering are also still observed, although the corrugation is reduced compared to pristine graphene.

Once atomic H is produced via field dissociation, hydrogenation of the graphene can take several hours after the sample is cooled back down to 5 K, which provides insight into the growth mechanism. The graphene island in Figure 2a showed no evidence of hydrogenation ~1.5 hrs after the field dissociation and 20 K anneal cycle. However, domains of hydrogenated graphene (H-Gr) were observed one hour later, evidenced by the $\sqrt{3} \times \sqrt{3}R30^\circ$ structure in the atomic resolution STM image and corresponding FFT in Fig. 2b. The domain boundaries are mobile, and H-Gr

patches can move, grow or shrink, with time and/or repeated STM imaging. Such patches appear to be ~ 0.2 Å lower than the surrounding graphene in STM images, suggesting a suppression of conductivity under these tunneling conditions. Complete hydrogenation was observed ~ 20 min after taking the image in Fig. 2b, and only the H-Gr lattice was observed in both real space and FFT images (Fig. 2c).

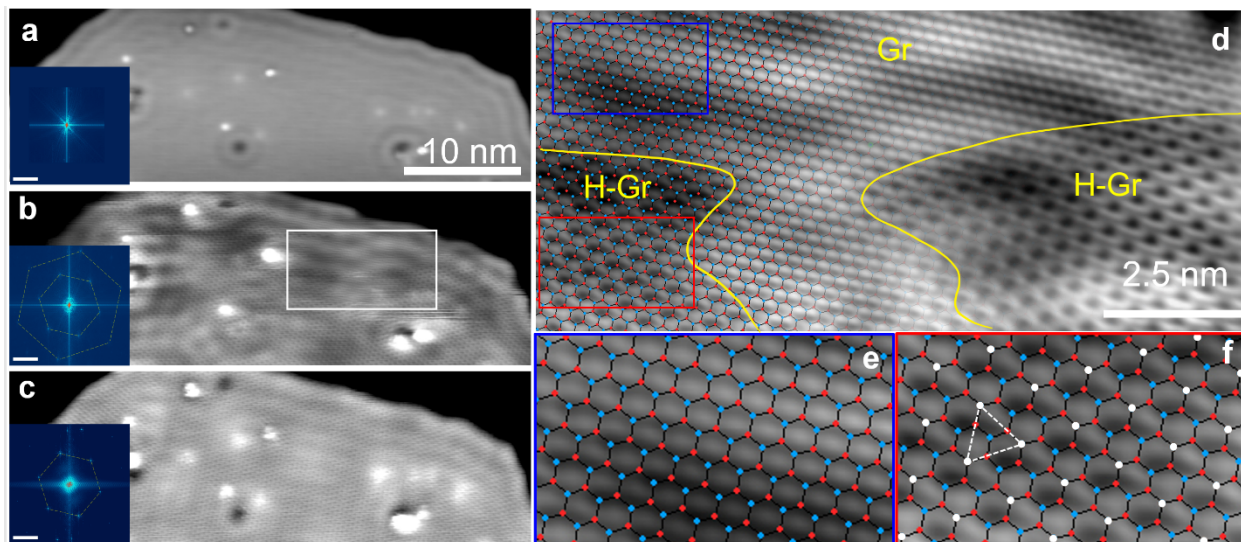


Figure 2. Growth dynamics and assignment of hydrogenated graphene lattice. (a) STM image of a graphene area showing no hydrogenation after the process in Fig. 1(a). (b) STM image of the island taken an hour later, showing domains of pristine and hydrogenated graphene. The FFT inset shows two hexagons corresponding to the graphene honeycomb lattice and the hydrogenated graphene lattice with $\sqrt{3} \times \sqrt{3}$ R30° reconstruction. (c) STM image taken 20 minutes after (b). Only hydrogenated graphene is now observed in both real-space and FFT images. (d) Magnified view of the area in (b) indicated by the white rectangle with a graphene honeycomb lattice overlay. This area shows both the pristine graphene lattice and hydrogenated graphene lattice as indicated in the image. (e-f) Further magnified views ($3 \times 1.5 \text{ nm}^2$) of pristine (e) and hydrogenated (f) graphene areas indicated by the rectangles in (d). In (f), hydrogen atoms are marked by the white dots and the unit cell of the hydrogenated graphene lattice is marked by the white triangle. ($V = 1.0\text{V}$, $I = 0.2\text{nA}$) for (a), ($V = 50\text{mV}$, $I = 0.2\text{nA}$) for (b) – (f). FFT scale bars = 2.0 nm^{-1} .

We attribute these growth dynamics to the mobility of atomic hydrogen on the surface and stability against associative desorption as H_2 . Previous studies demonstrated quantum tunneling of chemisorbed H on Cu(100), which leads to appreciable motion even at 5 K. More recent STM studies of H on Cu(111) showed similar behavior, and even a tendency to cluster³⁴. The progression of hydrogenation in Figure 2 suggests that excess H produced via field dissociation migrates on the surface until bonding to the carbon atoms in the graphene island. The long-time scale behavior would indicate that while the high-energy field emission electrons are needed to break the H-H bond of physisorbed H_2 , this energy is not needed for H to bond to the C atoms in graphene. It seems that the thermal energy at 5 K, or quantum effects, are sufficient to produce the subsequent hydrogenation of graphene.

The images in Fig. 2 confirm that the 4.3 Å lattice cannot be an artifact of the tip termination, as both graphene and hydrogenated graphene lattices are reproducibly resolved in the same scan line. Images of these coexisting domains help in the registry of the graphene and H-Gr lattices (Fig. 2d-f). For the pristine graphene region, we observed a triangular lattice of bright protrusions with a spacing of 2.5 Å, consistent with the spacing between hexagon centers in graphene (Fig. 2e)²⁶. Thus, although the individual carbon atoms were not resolved with this STM tip termination, we can construct an overlay of the graphene lattice and extend this overlay onto the H-Gr regions. Prior work suggests that H adatoms on graphene are imaged as three-fold symmetric protrusions^{11,19,22,35}. Following this assignment, we locate the hydrogen atoms in the H-Gr regions as shown by the white dots in Fig. 2f, with the unit cell as indicated by the white triangle. The hydrogenated graphene area shows a $\sqrt{3} \times \sqrt{3}R30^\circ$ reconstruction with respect to the graphene lattice, with hydrogen atoms on only one of the C sublattices.

Recently, Lin et al., reported small ($\sim \text{nm}^2$) patches of the $\sqrt{3}$ structure coexisting with other ordered structures on Gr/Cu foil, and DFT calculations which suggested this was not the lowest energy structure²². While we have observed other structures (c.f., Figure 4), we predominately observe the $\sqrt{3}$ structure, which extends over much larger areas in our study (e.g. $>3000 \text{ nm}^2$ in Fig. 1c). One possible explanation is that the thermodynamic conditions in the two methods are quite different. The typical thermal cracking method used by Lin et al., results in a flux of highly energetic, reactive H onto the surface, which is held at room temperature. Here, we produce H *in situ* at 5 K, and the hydrogenation proceeds at low temperature.

To probe the hydrogen-graphene interaction and resultant changes in electronic structure, we performed tunneling spectroscopy across a domain boundary between H-Gr and graphene (Fig. 3a). Spectra taken on graphene (Fig. 3b, blue curve) show a step at -0.3 V which we attribute to the Cu(111) surface state band edge, shifted by +0.1 V due to the graphene overlayer²⁶. Consistent with other studies of graphene on metal surfaces^{19,26-28,36-38}, the Dirac point is not evident, likely due to the high conductivity of the underlying Cu. On H-Gr, we observed a $\sim 20\%$ decrease in conductivity over a $\sim 0.5\text{V}$ range, and this was characteristic for spectra taken at different points in the H-Gr patch. The Cu(111) surface state band edge shows no further shift on H-Gr, but the onset is suppressed in comparison to data taken on Gr. This observation is consistent with the STM

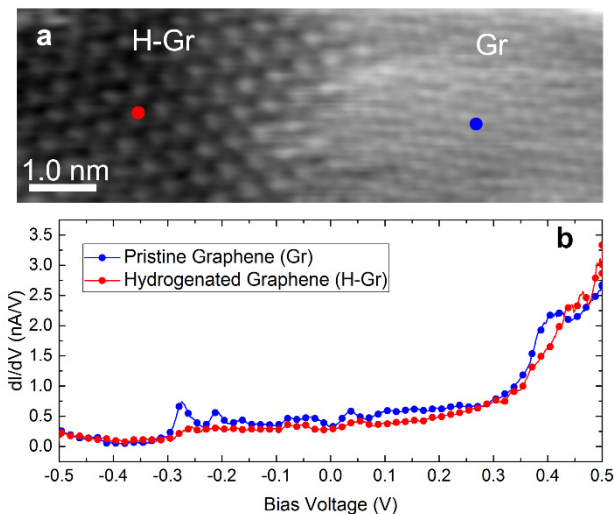


Figure 3. Scanning tunneling spectroscopy comparison of pristine and hydrogenated graphene. (a) STM image showing a domain boundary between hydrogenated and pristine graphene. ($V = 0.5\text{V}$, $I = 0.2\text{nA}$). (b) dI/dV spectroscopy of pristine (blue) and hydrogenated (red) graphene at locations marked by circles in (a). The tip height was set at (0.5 V, 0.51 nA) before disabling the STM feedback loop.

imaging in Figure 1d, where we observed a lower amplitude corrugation from the Shockley surface state scattering in the real-space image, and a fainter ring in the FFT.

A number of DFT studies have explored how the band gap opening on hydrogenated graphene depends on the hydrogen coverage and single/double sided termination^{39–42}. The wide 3.5 eV gap for graphane²⁴ is predicted to be reduced to ~ 0.6 eV for the $\sqrt{3} \times \sqrt{3}$ R30° structure⁴². Experimentally, Lin et al. observed gaps ranging from 0.6 to 1.2 eV on H-Gr regions, and a V-shaped feature on graphene regions attributed to the Dirac point²². It is likely that the more pristine interface in our UHV-grown samples leads to a greater masking of the graphene and H-Gr electronic structure by the underlying Cu(111) substrate. Thus, although the predicted bandgap is qualitatively similar to the range of suppressed conductance in Fig. 3b, further study on other substrates is needed to isolate the H-Gr electronic structure.

Different structures of hydrogenated graphene were also observed. The STM image in Figure 4b shows two regions with triangular lattice spacings of 7.8 Å and 10.1 Å, corresponding to 3x3 and 4x4 reconstructions. In both domains, the Moiré pattern seen in the pristine graphene (Figure 4a) is no longer observed, in contrast to Figs. 1c,d for the $\sqrt{3}$ structure. The reconstructions in Figure 4 correspond to a less dense packing of the hydrogen, suggesting that factors such as the initial H₂ coverage and/or field emission profile of the STM tip may influence the hydrogenation process.

Similar to a previous study¹¹, we find that the graphene hydrogenation is reversed by imaging with higher bias voltage (>4.5 V) compared to typical imaging conditions (<1 V). As we repeatedly imaged the area in Figure 4 with higher bias (not shown), the Moiré pattern from the pristine graphene gradually re-emerged. After switching back to typical imaging conditions (Fig. 4c), the 3x3 and 4x4 reconstructions were no longer observed, and the pristine graphene was recovered, with a few additional point defects.

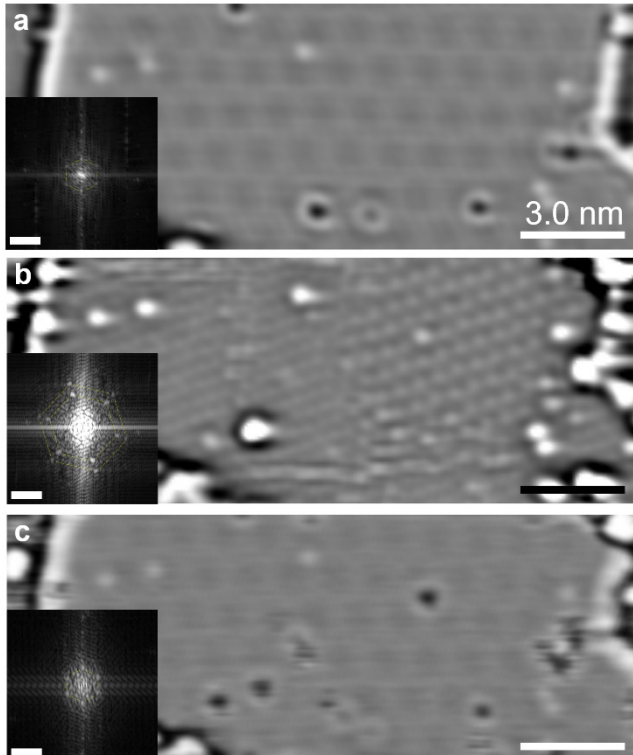


Figure 4. Reversibility of graphene hydrogenation. (a) Laplace filtered STM image of pristine graphene showing point defects and Moiré pattern. (inset) FFT showing hexagonal spots corresponding to the Moiré pattern (b) Image after the hydrogenation process, showing two regions with triangular lattice spacings corresponding to 3x3 (left) and 4x4 (right) reconstructions. (Inset) FFT showing corresponding hexagonal spot patterns (c) After imaging with high bias voltage (> 4.5 V), the 3x3 and 4x4 reconstructions are no longer observed and the pristine graphene Moiré pattern is recovered. (Inset) FFT showing the same Moiré pattern as in (a). $V = 1$ V, $I = 0.2$ nA. FFT scale bar = 2.0nm^{-1} .

In contrast to previous hydrogenation efforts via thermal cracking of H₂, our field dissociation method produces crystalline ordering within the relatively large, micron-scale field emission profile of the STM tip. Furthermore, only one sublattice is occupied, which may yield novel magnetic phases³⁵. While local and reversible hydrogenation of graphene is a promising avenue for tuning graphene's properties, further study is needed to understand the nature of the H-graphene bond. The mobility of domain boundaries (Figs. 2,3) and reversibility (Fig. 4) is more characteristic of a weakly bound adsorbate system, and would be somewhat surprising if covalent C-H bonding were present. The light mass of hydrogen however, suggests that diffusion on graphene via quantum tunneling is likely, which may underlie these dynamics. Recent theoretical studies have suggested such diffusion processes are possible⁴³. We also cannot rule out the influence of physisorbed H₂, which may remain on the surface despite our annealing procedure. The phase diagram of H₂ on graphite does show a commensurate $\sqrt{3}$ phase⁴⁴, but in our experiments, the structures reported here did not occur in the absence of field dissociation. Further studies of hydrogenated graphene on SiO₂ or h-BN could provide insight into these questions by better disentangling the intrinsic electronic structure of H-Gr from that of the substrate.

Acknowledgement

Funding for this research was provided by the Center for Emergent Materials at the Ohio State University: an NSF MRSEC under award number DMR-1420451.

References

- (1) Ferrari, A. C.; Bonaccorso, F.; Fal'ko, V.; Novoselov, K. S.; Roche, S.; Bøggild, P.; Borini, S.; Koppens, F.; Palermo, V.; Pugno, N.; Garrido, J. a.; Sordan, R.; Bianco, A.; Ballerini, L.; Prato, M.; Lidorikis, E.; Kivioja, J.; Marinelli, C.; Ryhänen, T.; Morpurgo, A.; Coleman, J. N.; Nicolosi, V.; Colombo, L.; Fert, A.; Garcia-Hernandez, M.; Bachtold, A.; Schneider, G. F.; Guinea, F.; Dekker, C.; Barbone, M.; Galiotis, C.; Grigorenko, A.; Konstantatos, G.; Kis, A.; Katsnelson, M.; Beenakker, C. W. J.; Vandersypen, L.; Loiseau, A.; Morandi, V.; Neumaier, D.; Treossi, E.; Pellegrini, V.; Polini, M.; Tredicucci, A.; Williams, G. M.; Hong, B. H.; Ahn, J. H.; Kim, J. M.; Zirath, H.; van Wees, B. J.; van der Zant, H.; Occhipinti, L.; Di Matteo, A.; Kinloch, I. a.; Seyller, T.; Quesnel, E.; Feng, X.; Teo, K.; Rupesinghe, N.; Hakonen, P.; Neil, S. R. T.; Tannock, Q.; Löfwander, T.; Kinaret, J. *Nanoscale* **2014**, 7 (11), 4598–4810.
- (2) Novoselov, K. S.; Fal'ko, V. I.; Colombo, L.; Gellert, P. R.; Schwab, M. G.; Kim, K. *Nature* **2012**, 490 (7419), 192–200.
- (3) Ryu, S.; Han, M. Y.; Maultzsch, J.; Heinz, T. F.; Kim, P.; Steigerwald, M. L.; Brus, L. E. *Nano Lett.* **2008**, 8 (12), 4597–4602.
- (4) Jones, J. D.; Mahajan, K. K.; Williams, W. H.; Ecton, P. A.; Mo, Y.; Perez, J. M. *Carbon N. Y.* **2010**, 48 (8), 2335–2340.
- (5) Woo, S. O.; Teizer, W. *Appl. Phys. Lett.* **2013**, 103 (4), 041603.
- (6) Whitener Jr, K. E.; Lee, W. K.; Campbell, P. M.; Robinson, J. T. *Carbon N. Y.* **2014**, 72, 348–353.
- (7) Ruffieux, P.; Gröning, O.; Schwaller, P.; Schlapbach, L.; Gröning, P. *Phys. Rev. Lett.*

- 2000**, *84* (21), 4910–4913.
- (8) Elias, D. C.; Nair, R. R.; Mohiuddin, T. M. G.; Morozov, S. V.; Blake, P.; Halsall, M. P.; Ferrari, A. C.; Boukhvalov, D. W.; Katsnelson, M. I.; Geim, A. K.; Novoselov, K. S. *Science* **2009**, *323* (5914), 610–613.
 - (9) Xie, L.; Wang, X.; Lu, J.; Ni, Z.; Luo, Z.; Mao, H.; Wang, R.; Wang, Y.; Huang, H.; Qi, D.; Liu, R.; Yu, T.; Shen, Z.; Wu, T.; Peng, H.; Özyilmaz, B.; Loh, K.; Wee, A. T. S.; Ariando; Chen, W. *Appl. Phys. Lett.* **2011**, *98* (19), 193113.
 - (10) Jayasingha, R.; Sherehiy, A.; Wu, S.-Y.; Sumanasekera, G. U. *Nano Lett.* **2013**, *13* (11), 5098–5105.
 - (11) Sessi, P.; Guest, J. R.; Bode, M.; Guisinger, N. P. *Nano Lett.* **2009**, *9* (12), 4343–4347.
 - (12) Balog, R.; Jørgensen, B.; Wells, J.; Lægsgaard, E.; Hofmann, P.; Besenbacher, F.; Hornekær, L. *J. Am. Chem. Soc.* **2009**, *131* (25), 8744–8745.
 - (13) Guisinger, N. P.; Rutter, G. M.; Crain, J. N.; First, P. N.; Stroschio, J. A. *Nano Lett.* **2009**, *9* (4), 1462–1466.
 - (14) Bostwick, A.; McChesney, J. L.; Emtsev, K. V.; Seyller, T.; Horn, K.; Kevan, S. D.; Rotenberg, E. *Phys. Rev. Lett.* **2009**, *103* (5), 056404.
 - (15) Haberer, D.; Vyalikh, D. V.; Taioli, S.; Dora, B.; Farjam, M.; Fink, J.; Marchenko, D.; Pichler, T.; Ziegler, K.; Simonucci, S.; Dresselhaus, M. S.; Knupfer, M.; Büchner, B.; Grüneis, A. *Nano Lett.* **2010**, *10* (9), 3360–3366.
 - (16) Ng, M. L.; Balog, R.; Hornekær, L.; Preobrajenski, A. B.; Vinogradov, N. A.; Mårtensson, N.; Schulte, K. *J. Phys. Chem. C* **2010**, *114* (43), 18559–18565.
 - (17) Balog, R.; Jørgensen, B.; Nilsson, L.; Andersen, M.; Rienks, E.; Bianchi, M.; Fanetti, M.; Laegsgaard, E.; Baraldi, A.; Lizzit, S.; Slijivančanin, Z.; Besenbacher, F.; Hammer, B.; Pedersen, T. G.; Hofmann, P.; Hornekaer, L. *Nat. Mater.* **2010**, *9* (4), 315–319.
 - (18) Katoch, J.; Chen, J. H.; Tsuchikawa, R.; Smith, C. W.; Mucciolo, E. R.; Ishigami, M. *Phys. Rev. B* **2010**, *82* (8), 081417.
 - (19) Scheffler, M.; Haberer, D.; Petaccia, L.; Farjam, M.; Schlegel, R.; Baumann, D.; Hänke, T.; Grüneis, A.; Knupfer, M.; Hess, C.; Büchner, B. *ACS Nano* **2012**, *6* (12), 10590–10597.
 - (20) Ziatdinov, M.; Fujii, S.; Kusakabe, K.; Kiguchi, M.; Mori, T.; Toshiaki, E. *Phys. Rev. B* **2014**, *89* (15), 155405.
 - (21) Zhao, W.; Gebhardt, J.; Späth, F.; Gotterbarm, K.; Gleichweit, C.; Steinrück, H. P.; Görling, A.; Papp, C. *Chem. - A Eur. J.* **2015**, *21* (8), 3347–3358.
 - (22) Lin, C.; Feng, Y.; Xiao, Y.; Dürr, M.; Huang, X.; Xu, X.; Zhao, R.; Wang, E.; Li, X.-Z.; Hu, Z. *Nano Lett.* **2015**, *15*, 903–908.
 - (23) Jørgensen, J. H.; Čabo, A. G.; Balog, R.; Kyhl, L.; Groves, M. N.; Cassidy, A. M.; Bruix, A.; Bianchi, M.; Dendzik, M.; Arman, M. A.; Lammich, L.; Pascual, J. I.; Knudsen, J.; Hammer, B.; Hofmann, P.; Hornekaer, L. *ACS Nano* **2016**, DOI: 10.1021/acsnano.6b04671.
 - (24) Sofo, J. O.; Chaudhari, A. S.; Barber, G. D. *Phys. Rev. B* **2007**, *75* (15), 153401.
 - (25) Wen, X.; Hand, L.; Labet, V.; Yang, T.; Hoffmann, R.; Ashcroft, N. W.; Oganov, A.; Lyakhov, A. *Proc. Natl. Acad. Sci. U. S. A.* **2011**, *108* (17), 6833–6837.
 - (26) Hollen, S. M.; Gambrel, G. A.; Tjung, S. J.; Santagata, N. M.; Johnston-Halperin, E.; Gupta, J. A. *Phys. Rev. B* **2015**, *91* (19), 195425.
 - (27) Hollen, S. M.; Tjung, S. J.; Mattioli, K. R.; Gambrel, G. A.; Santagata, N. M.; Johnston-Halperin, E.; Gupta, J. A. *J. Phys. Condens. Matter* **2016**, *28* (3), 034003.

- (28) Gao, L.; Guest, J. R.; Guisinger, N. P. *Nano Lett.* **2010**, *10* (9), 3512–3516.
- (29) Horcas, I.; Fernández, R.; Gómez-Rodríguez, J. M.; Colchero, J.; Gómez-Herrero, J.; Baro, A. M. *Rev. Sci. Instrum.* **2007**, *78* (1), 013705.
- (30) Gupta, J.; Lutz, C.; Heinrich, a.; Eigler, D. *Phys. Rev. B* **2005**, *71* (11), 115416.
- (31) Kammler, T.; Küppers, J. *J. Chem. Phys.* **1999**, *111* (17), 8115–8123.
- (32) Jewell, A. D.; Peng, G.; Mattera, M. F. G.; Lewis, E. A.; Murphy, C. J.; Kyriakou, G.; Mavrikakis, M.; Sykes, E. C. H. *ACS Nano* **2012**, *6* (11), 10115–10121.
- (33) Lauhon, L.; Ho, W. *Phys. Rev. Lett.* **2000**, *85* (21), 4566–4569.
- (34) Hornekær, L.; Rauls, E.; Xu, W.; Šljivančanin, Ž.; Otero, R.; Stensgaard, I.; Lægsgaard, E.; Hammer, B.; Besenbacher, F. *Phys. Rev. Lett.* **2006**, *97* (18), 186102.
- (35) González-Herrero, H.; Gómez-Rodríguez, J. M.; Mallet, P.; Moaied, M.; Palacios, J. J.; Salgado, C.; Ugeda, M. M.; Veuillen, J.-Y.; Yndurain, F.; Brihuega, I. *Science* **2016**, *352* (6284), 437–441.
- (36) Marchini, S.; Günther, S.; Wintterlin, J. *Phys. Rev. B* **2007**, *76* (7), 75429.
- (37) Feng, W.; Lei, S.; Li, Q.; Zhao, A. *J. Phys. Chem. C* **2011**, *115* (50), 24858–24864.
- (38) Wintterlin, J.; Bocquet, M. L. *Surf. Sci.* **2009**, *603* (10–12), 1841–1852.
- (39) García-Lastra, J. M. *Phys. Rev. B* **2010**, *82* (23), 235418.
- (40) Farjam, M.; Haberer, D.; Grüneis, A. *Phys. Rev. B* **2011**, *83* (19), 193411.
- (41) Grassi, R.; Low, T.; Lundstrom, M. *Nano Lett.* **2011**, *11* (11), 4574–4578.
- (42) Mirzadeh, M.; Farjam, M. *J. Phys. Condens. Matter* **2012**, *24* (23), 235304.
- (43) Talbot, J.; LeBohec, S.; Mishchenko, E. G. *Phys. Rev. B* **2016**, *93* (11), 115402.
- (44) Wiechert, H. Dynamics of H₂, HD, D₂ monolayers physisorbed on graphite. In *Physics of Covered Solid Surfaces · Adsorbed Layers on Surfaces* [Online]; Bonzel, A. P., Ed.; Springer, 2003; Vol. 42A3, pp 242–282. <http://materials.springer.com/bp/docs/978-3-540-45849-4> (accessed November 3, 2016).